

Diffusion of Buffer Layer Assisted Grown Gold Nanoclusters on Ru(100) and p(1 × 2)-O/Ru(100) Surfaces

Gabriel Kerner, Yonatan Horowitz, and Micha Asscher*

Department of Physical Chemistry, The Farkas Center for Light Induced Processes,
The Hebrew University of Jerusalem, Jerusalem 91904, Israel

Received: September 28, 2004; In Final Form: January 9, 2005

Patterning of metallic clusters on surfaces is demonstrated by utilizing a buffer layer assisted laser patterning technique (BLALP). This method has been employed in order to measure the diffusion of AFM and STM characterized size selected gold nanoclusters (5–10 nm diameter), over Ru(100) and p(1 × 2)-O/Ru(100) surfaces. Optical linear diffraction from gold cluster coverage gratings was utilized for the macroscopic diffusion measurements. The clusters were found to diffuse on the surface intact without significant coalescence or sintering. The barrier for metastable gold nanocluster diffusion on the surface is thought to be lower than the energy required for surface wetting. The apparent activation energy for diffusion was found to depend on the cluster size, increasing from 6.2 ± 0.4 kcal/mol for 5 nm clusters to 10.6 ± 0.5 kcal/mol for 9 nm clusters. The macroscopic diffusion of gold nanoclusters has been studied on the p(1 × 2)-O/Ru(100) surface as well, where surface diffusion was found to be rather insensitive to the clusters size with activation energy of 5.5 ± 1 kcal/mol. The difference between the two surfaces is discussed in terms of a better commensurability (higher level of friction) of the gold facets at the contact area with the clean Ru(100) than in the case of the oxidized surface.

1. Introduction

Supported nanoclusters of noble metals are important in modern heterogeneous catalysis for their outstanding reactivity, their very high efficiency and the wide range of their applications.^{1–23} For example, nanoscale gold particles dispersed over an oxide support exhibit remarkable catalytic activity, in contrast to the inert nature of gold as bulk material.^{2,17–22} In fact, it is claimed to be among the most effective catalysts for the low-temperature CO oxidation reaction.^{8–10}

However, application under realistic industrial conditions of high pressure and temperature is often tempered by the tendency of supported metallic clusters to sinter and coalesce.^{8–18} Cluster coalescence on solid substrates is rather sensitive to the nature of the support material.^{1–10,21–22} Moreover, cluster–support interactions may enhance or quench reactivity and selectivity of a catalyst. To be able to limit coalescence phenomena toward sintering resistant catalysts, a basic understanding of cluster formation and diffusion is required.^{14–17}

Growth of 3D islands on solid surfaces is a result of delicate interplay between the substrate surface free energy and that of the clusters' material.⁴ Recently, Weaver and co-workers have developed the buffer layer assisted growth (BLAG) process to form and deposit well-defined clusters on surfaces, to study their size dependent properties.^{24–30} The BLAG procedure avoids much of the constraints of surface free energy regarding 3D growth mode. The metal to be deposited is spread over a physisorbed buffer layer of xenon. Desorption of the buffer atoms leads to “soft landing” of the metal and its deposition on the surface as clusters, whose size depends on the buffer layer thickness. BLAG is not limited to the growth of metallic clusters as was recently demonstrated when Ge nanoclusters were deposited on Si by employing the BLAG method.^{28b}

In this paper we shall utilize the BLAG process to deposit uniform size and lateral distribution of gold nanoclusters on a well-defined Ru(100) surface. Thermal stability of such metallic nanoclusters is of fundamental importance for better understanding and control of sintering or cluster coalescence, which is among the most problematic problems pertaining to catalyst aging and reduced reactivity known under realistic industrial conditions.

Macroscopic diffusion measurements can be performed by following in real time the smearing out of a periodic coverage modulation.^{31–44} This is performed by interfering two laser beams to form a coverage grating using Laser-induced thermal desorption (LITD).^{32–38} Then, by optical diffraction methods (second harmonic^{34,41–44} or linear^{31–32,38–40}), one follows the decay of high order diffractions in real time at diffusion temperatures. This method has been employed for surface diffusion studies, but it was limited to weakly bound adsorbates on surfaces. Adsorbed metal atoms are typically strongly chemisorbed to the substrate. Creating a coverage grating of metallic clusters on surfaces, therefore, by direct LITD of the substrate would require an extremely high laser power that would exceed surface damage threshold in most metal/substrate systems.

In this work we have employed the buffer layer assisted laser patterning (BLALP) recently developed in our laboratory in order to form a metallic (or any other material) coverage grating.^{45–46} Once cluster coverage grating has been established, thermal stability and diffusion were followed in real time using optical linear diffraction, as a function of clusters average size. Substrate effect on cluster diffusion was studied as well by comparing the results over clean Ru(100) vs the oxygen covered p(1 × 2)-O/Ru(100) surface. The significance of these direct

measurements for sintering and cluster coalescence under realistic industrial conditions is discussed.

2. Experimental Section

The details of the experimental setup were given elsewhere.^{45,50} Briefly, measurements were performed in a UHV chamber, with base pressure of 3×10^{-10} mbar. The Ru(100) substrate was mounted on a cryogenic cold head (ADP Inc.) and held at 20 K. The sample was attached to the cold head by two tantalum wires (0.5 mm diameter), that were also used for resistively heating the sample. A W26Re–W5Re thermocouple spot-welded to the edge of the sample was employed to determine the sample's temperature.^{47,48} The sample was periodically cleaned by 600 eV Ne⁺ sputter and before each measurement it was also thermally annealed to 1620K.⁴⁹ The Ru(100) substrate oriented within 0.1% of the indicated plane was checked by LEED for its long range order. A sharp rectangular $p(1 \times 1)$ pattern was regularly obtained following the standard cleaning/annealing procedure. An ordered oxygen covered Ru(100) surface was prepared by annealing the surface to 600 K for 4 min at an oxygen pressure of 10^{-7} mbar. The sample was then flash heated to 1000 K at the base pressure, to remove excess oxygen from the surface, resulting in a sharp $p(1 \times 2)$ LEED pattern. The sputter cleaning and oxidation procedures were performed before each measurement, to make sure that no carbon contaminants or gold residues remained on the surface. Here, 99.995% pure Xe was used for the buffer layer growth. It was deposited on the sample at 20 K by backfilling the vacuum chamber to Xe pressures of up to 5×10^{-8} mbar, for exposure times necessary to obtain Xe layers at thicknesses between 10 and 100ML. The sticking probability of Xe at 20 K was assumed to be unity; therefore, exposure of 4L was considered equivalent to 1ML. Total exposure was calibrated with the actual Xe thickness by temperature-programmed desorption (TPD) experiments.⁵⁰ Gold atoms were deposited onto the Xe buffer layer in a vacuum, by resistively heating a tungsten wire wrapped around a 1 mm diameter Au wire (99.99% pure). The gold wire was melted and thoroughly degassed prior to use. Metal evaporation flux was monitored using a quartz microbalance, in units of Å/s. The typical evaporation rate was 0.05 Å/s. The structure and size distribution of the gold clusters formed via BLAG were determined ex situ under ambient conditions using STM and AFM.

A p-polarized pulsed Nd:YAG laser at its fundamental wavelength of 1064 nm, having a pulse duration of 10 ns, was used for metallic cluster coverage grating formation employing LITD. This was performed by interfering two split beams originated from the same pulse on the surface at incidence angle of 7.5°. This has led to the formation of a coverage grating having a period of 4 μm. The absorbed laser power used for desorption of the Xe physisorbed buffer layer and the metallic film on top was limited to 3MW/cm², avoiding any risk of surface damage by the pulsed laser heating.^{45,46}

3. Results and Discussion

3.1. Cluster Growth via Buffer Layer. Gold cluster growth via the BLAG method²⁴ was reproduced here prior to its laser patterning. Pure gold was vacuum deposited over multilayer xenon at different layer thicknesses on the Ru substrate, held at 20 K. The surface was then thermally annealed to 100 K at a heating rate of 1 K/s, to remove the physisorbed Xe. This annealing activates cluster diffusion, aggregation, and coalescence within the subliming buffer layer while descending toward the ruthenium substrate. The average size of the produced

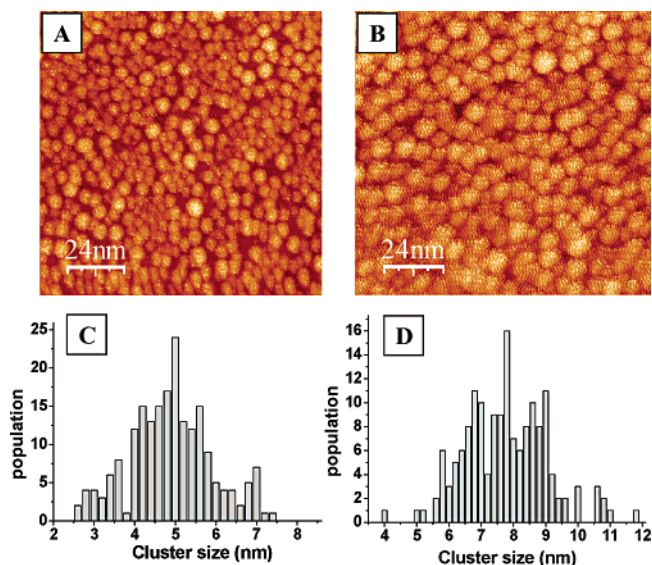


Figure 1. STM images of gold nanoclusters on Ru(100) deposited via the buffer layer assisted growth (BLAG) method, using the following parameters: (A) 1 nm of Au on 20ML xenon; (B) 2.3 nm Au on 30ML Xe. The histograms represent the corresponding dispersion of the gold cluster sizes on the surface.

nanostructures can be controlled and varied by suitable choice of the buffer layer thickness and quantity of metallic element evaporated on top.²⁷ The gold nanostructures prepared this way were found to be very stable after exposure to air at ambient conditions. No change was observed in cluster size or density of samples stored in air for several days. In Figure 1, parts A and B, STM images are shown of gold clusters deposited in a vacuum on the bare Ru(100) surface. The images were subsequently taken in air. Size distribution histograms were obtained by counting the number of particles within a certain size range, as demonstrated in Figure 1, part C and D.

STM tip effects may distort the actual particles size and in particular their lateral dimensions (unlike height which is considered to be accurate to better than 0.3 Å). Tip effects are considered particularly serious in lateral size determination using AFM imaging. To accurately correlate between the height and base radius (footprint) of the clusters, samples consisting of gold clusters grown via identical BLAG procedure on a SiO₂/Si-(100) substrate were examined ex situ utilizing a high resolution SEM and AFM. The clusters were found to be roughly hemispherical, having height-to-base ratio close to unity (on average) for clusters diameter above 4 nm. In all subsequent AFM measurements, the size of a given cluster was determined by measuring its height and assuming a hemispherical shape.

The size distribution of the deposited clusters has a typical width (at half-maximum) of 20%, in accordance with previously reported studies of the same procedure.^{25–28a} For a certain equivalent gold layer thickness, the average cluster size increases with the xenon buffer layer thickness, up to 60ML of Xe. This is shown in Figure 2. For 1 nm of gold evaporated on top of 20ML Xe, the average cluster diameter finally deposited on the Ru substrate is 5 nm, with a density of about 2×10^{12} clusters/cm². Evaporating the same amount of gold on 60ML Xe, the average cluster diameter grows to 9 nm, while cluster density decreases to about 3×10^{11} clusters/cm². The full width at half-maximum of the cluster size distribution (fwhm) increases accordingly from 1.8 to 2.2 and 2.4 nm for average cluster diameters of 5, 7.5, and 9 nm, respectively. The cluster size depends also on the amount of evaporated gold on the buffer layer. This is demonstrated in Figure 1B where Xe layer

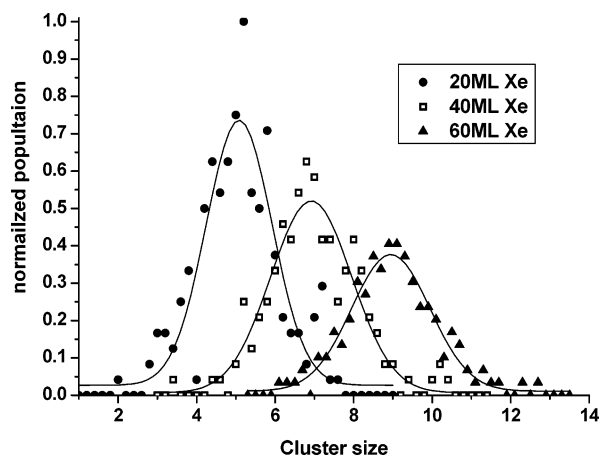


Figure 2. Average cluster size and distribution of the Au nanoclusters formed by deposition of 1 nm Au on a xenon buffer layer, following annealing to room temperature, for different buffer layer thicknesses.

thickness of only 30ML is enough to form average clusters size of 7.5 nm upon evaporation of 2.3 nm equivalent gold on top of the buffer layer. So 30ML Xe with 1 nm of deposited gold would result in average size of 6 nm only. Similar densities were obtained in a recent study of the growth of Fe clusters (nanodots) on Cu(111) using BLAG.^{28c}

In direct deposition of metals on oxide surfaces, the cluster size depends on the substrate temperature, the evaporation rate and it strongly depends on the strength of the interaction with the substrate. In contrast, the BLAG method can be used to form a wide range of cluster sizes on any desired substrate, with a reasonable control over the size distribution. The results presented here differ somewhat from those recently reported by Weaver and co-workers.^{27–30} In our study, the cluster's shape, height, and diameter were characterized to be of compact morphology, employing STM and AFM imaging. These results are similar to previous study by Weaver et al. where BLAG was used to deposit Au and Ag particles on Si surfaces.^{24–26} However, our data suggest higher cluster density on the substrate. This may arise from more deposited gold on the buffer layer typical to our study. In addition, slight differences are expected since substrate temperature and buffer thickness determination vary in different laboratories and therefore may lead to slight differences in the final cluster density.

It is interesting to note, however, that when BLAG generated gold clusters are deposited on graphite, ramified and fractal-like structures were observed by employing TEM analysis. The origin of these different shapes is not yet fully understood.

3.2. Coverage Grating via BLALP. As described in previous publications,^{45,46} cluster density can be modulated by employing the BLALP technique to form coverage grating of clusters of different sizes. By monitoring He–Ne diffraction intensity at various substrate temperatures, cluster diffusion can be studied. Figure 3 demonstrates an AFM image⁶² of gratinglike coverage modulation, of 4.5 nm average height Au particles, BLAG formed by evaporating 1 nm of gold via 60ML xenon. As expected the grating pattern is composed of high density clusters, relatively uniform in size. The bright spots observed in the clean areas of the grating troughs are rather large metal particles that have not been ejected by the xenon during the desorbing laser pulse. Their origin is yet unclear; however, they may be caused by micrometer range crystallite areas of the xenon buffer layer, as proposed by Antonov et al.²⁹

Annealing the sample in air to 600 K for 2 h has affected neither the pattern nor the average cluster size. It is believed

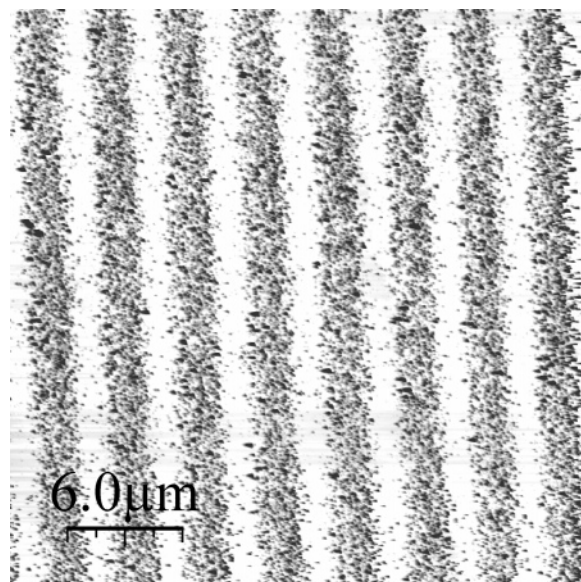


Figure 3. AFM image (in air) of a coverage modulation of gold clusters formed via the, buffer layer assisted laser patterning (BLALP) procedure. The grating period is of 4 μm .

that deep oxidation of the substrate anchors the clusters, thus avoiding any diffusion or sintering of these particles. However, creating the same coverage modulation and annealing in a vacuum to 450 K at 3 K/s, followed by fast cooling back to 100 K, lead to cluster diffusion and to the diminishing of the optical linear diffraction pattern. After subsequent imaging of this sample with AFM, one discovers that although the clusters still dominate on the surface, they had diffused and smeared out the original periodic coverage modulation. This is demonstrated in Figure 4, parts A and B, for an average cluster height of 4.5 nm. Each AFM image represents an independent experiment, using same cluster growth parameters of 1 nm evaporated Au on 60ML xenon. The sample was extracted from the vacuum at a temperature of 200 K. This induced deep oxidation, i.e., “freezing” of the grating pattern, and avoids further diffusion of the clusters on the surface. Figure 4A represent the surface after deposition of the patterned clusters, but before any diffusion takes place. On the other hand, Figure 4B shows a snapshot of the surface during the diffusion of the clusters due to annealing to 450 K. Analysis of such an image reveals that cluster density modulation still exists to some extent on the surface, indicating that the diffusion process was not homogeneous nor has it been completed by annealing to this temperature. Repeating the patterning procedure and annealing in a vacuum to 550 K at 3 K/s led to the complete disappearance of the grating pattern and coverage modulation. Initial cluster density within the gold stripes (Figure 4A) is about 3×10^{11} clusters/cm², and it decreases to about two-thirds its initial value after diffusion (Figure 4B). The overall cluster density however (stripe with trough) remains constant within the experimental error, around 1.4×10^{11} clusters/cm². Cluster size distribution for both images is shown in Figure 4, parts C and D, respectively. The distribution is somewhat wider than previously measured with STM in Figure 2, maybe due to the tip effect, which induces the coalescence of some clusters. On the other hand, several large structures are observed. Their origin is yet unknown, however they are believed to form during desorption of the Xe buffer layer. One possible explanation is that occasionally several clusters sticks vertically to each other during the “soft landing” process, resulting in these large structures.

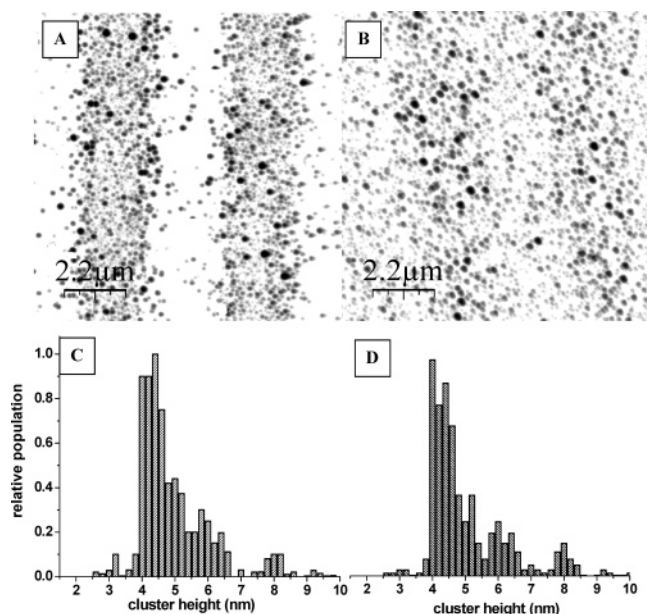


Figure 4. AFM images of a high-density gold cluster coverage grating created by BLALP: (A) after annealing in a vacuum to 300K and kept at room temperature; (B) after annealing to 450 K at 3 K/s in a vacuum, and quenched back to room temperature. (C and D) Cluster height distribution for parts A and B, respectively. One clearly observes the smearing out of the grating pattern, while cluster size distribution remains constant. The images were taken in air following the above in vacuo preparation and annealing procedures.⁶²

Few clusters with height below 1.5 nm could be found in both images. It is possible that coalescence of the smallest clusters occurs even below room temperature, thus are not detected in the AFM images. However, the overall cluster size distribution remains almost unchanged after annealing to 600 K at 3 K/s, as clearly shown by the cluster size distribution in Figure 4, parts C and D. This suggests that cluster coalescence and sintering are negligible at this temperature range, for clusters above 4 nm in size. On the other hand, cluster diffusion on the substrate is clearly observed. From the AFM images, it is deduced that smaller clusters are more mobile than the larger ones, suggesting size dependent activation energy for cluster diffusion, as will be discussed in more details below.

Gold nanocluster diffusion reported here and measured on the oxygen covered Ru surface as well (see below), is in contrast to gold directly grown on the clean Ru(100) and the oxygen covered Ru(100) surfaces, as shown in studies performed by Lambert and co-workers.^{63–64} Using AES and XPS methods, they showed that evaporation of gold atoms onto the clean metallic substrate (Ru(100)) favors a layered growth mode already at room temperature, while on the oxygen covered surface gold tends to agglomerate into three-dimensional structures, which gradually coalesce as temperature increases from about 400 to 1000 K.

This is a surprising result. Coalescence and sintering phenomena have been previously reported in the literature for gold nanoclusters on several other substrates such as TiO₂ and SiO₂, at a similar temperature range.^{8,17,21} Cluster diffusion mechanism in those systems was attributed to evaporation–condensation events, where atoms at the perimeter of small clusters detach and recondense on larger 3D islands.^{57–58} This process results in the expansion of large clusters at the expense of the smaller ones, generally resulting in a bimodal cluster size distribution on the substrate, also known as Ostwald ripening mechanism. Apparently, this is not the dominating process in the system of gold clusters gently deposited via BLALP on ruthenium discussed

here. Ultimately, the clusters are expected to evaporate/decompose and wet the metallic substrate underneath, as it is the most stable thermodynamic state for this system. In contrast, the fact that clusters appear in the grating trough clearly indicate that the cluster diffuses as a whole on the surface, at relatively low temperatures. The energy involved in the migration of the cluster is lower than that for 2D evaporation. As a result, clusters diffusion occurs at lower temperature than melting/wetting. It is possible that the surface energy of the already formed clusters kinetically hinders its decomposition, inducing a metastable state. Therefore, wetting of the surface by the gold atoms does not occur at temperatures below 600 K. Nevertheless, atomic evaporation and diffusion between the clusters may occur at this temperature range. A more detailed in situ microscopic study is required in order to confirm some of the predictions suggested above.

On the basis of the above discussion, we attempt to determine cluster size dependent diffusion kinetic parameters, as outlined below.

The diffusion of metal atoms and small clusters in homoepitaxial systems has been extensively studied.^{52–54} Fewer studies have dealt with heteroepitaxial systems.^{54–56,59} Moreover the diffusion of large 3D clusters on metallic and oxide surfaces is currently less well understood as those clusters were thought to be thermally stable. However, recent experimental evidence from STM studies^{57,58} have become available, showing that 2D Ag clusters (containing about 100 atoms) actually diffuse on Ag(100) substrates with similar results for Cu clusters on Cu-(100).⁵⁷ Similar behavior has been found for Pt 3D nanoclusters on the highly corrugated anatase TiO₂(100) surface.^{60–61} In these systems, cluster motion on surfaces is suggested to occur in a process taking place at the boundary of the clusters: peripheral diffusion (PD). In the PD process several types of atomic motions along the periphery of the cluster are responsible for the net displacement of the center-of-mass. However, the atoms do not leave the cluster while executing such movements.⁶⁷

The peripheral diffusion process is then suggested to be a possible mechanism for the migration of gold nanoclusters on the Ru(100) and the p(1 × 2)-O/Ru(100) surfaces. The energy barrier for the PD mechanism is expected to be smaller than the barrier for the diffusion–evaporation of atoms on the clusters or the substrate.^{40–42,53}

3.3. Temperature-Programmed Diffusion Method. Surface diffusion measurements over micrometer range distances are typically performed by monitoring the isothermal decay in time of the first-order linear diffraction peak originated from coverage grating formed by employing LITD^{31–44} or the BLALP method discussed above.^{45,46} For the case of BLALP generated gold cluster diffusion measurements, experimental conditions were those demonstrated in Figure 1 in terms of cluster size and distribution. The diffusion measurements were performed for two different gold dosages on the surface, 1 and 2.3 nm thickness equivalents as monitored by the quartz microbalance.

The one-dimensional Fick's diffusion equation for the simple case where the diffusion rate coefficient is coverage independent is given by

$$\frac{\partial \theta(x)}{\partial t} = D \frac{\partial^2 \theta(x)}{\partial x^2} \quad (1)$$

This is the diffusion equation and it has an analytical solution for the coverage $[\theta(x,t)]$ as a function of time. It can be transformed into the following expression for the linear diffracted signal intensity I_n :

$$I_n(t) = I_n(t=0)e^{-2\pi^2 n^2 D t/w^2} \quad (2)$$

Here n is the linear diffraction order, w is the coverage modulation period, and D is the temperature-dependent rate constant for diffusion: $D = D_0 \exp(-E_a/RT)$, where E_a is the activation energy for diffusion and D_0 is the preexponential factor. Recording the isothermal decay of the first-order linear diffraction, one should obtain the diffusion coefficient. From a plot of the diffusion coefficient vs the inverse temperature (Arrhenius analysis), the activation energy and preexponential factor for diffusion can be extracted.

In the present system, however, the diffusion of gold clusters on the Ru surface occurs over an exceptionally wide temperature range, about 250 K. Isothermal measurements become highly inefficient under such circumstances. Moreover, while heating the sample for a relatively long period of time (hundreds of seconds), e.g. for diffusion measurements below 400 K, the cold head and its surroundings gradually start to heat up and as a result lead to an undesired background pressure increase and to a slight thermal expansion instability. In contrast, continuously ramping the sample temperature avoids this thermal instability since it is a much faster process.

We introduce here a nonisothermal approach⁵¹ for diffusion measurements based on optical diffraction from one-dimensional coverage grating. The Fick second diffusion equation is used, by employing a correlation between the time (t) and the temperature (T) using a linear heating ramp

$$T = T_i + \beta t \quad (3)$$

where β is the heating rate in K/s.

The temperature dependent diffusion coefficient is not considered as constant anymore. Instead, its exponential dependence on temperature is explicitly considered. Solving eq 1, one obtains the following modification for eq 2:

$$\frac{I}{I_0} = e^{-a\beta \int_0^T D(T) dT} \quad (4)$$

where

$$a = \frac{2\pi^2 n^2}{w^2} \quad (5)$$

n is the n th optical linear diffraction order, and w is the coverage grating period, dictated by Bragg law. Expression 4 can be rewritten by inserting the Arrhenius expression for D :

$$\frac{I}{I_0} = e^{(-a/\beta)D_0(E_a/R)\int_0^T e^{RT/E_a} e^{1/\alpha} dx} \quad (6)$$

Note that the heating rate is embedded within the exponent in eq 6. Diffusion measurements utilizing surface temperature ramp and their respective fit using eq 6 above are shown in Figure 5. These are measurements of the diffusion of gold clusters on the clean Ru(100) substrate.

As an alternative to direct line shape analysis, the derivative of the plot in Figure 5 can be extracted as a function of the temperature.⁵¹ In this method, an expression for the decay of the observable $I_{(n=1)}$ is derived, to be subsequently related to parametrized values of the activation energy for diffusion (E_a):

$$\frac{\partial(I/I_0)}{\partial T} = \left(\frac{I}{I_0}\right) \left(-\frac{aD_0}{\beta} \cdot e^{-E_a/RT}\right) \quad (7)$$

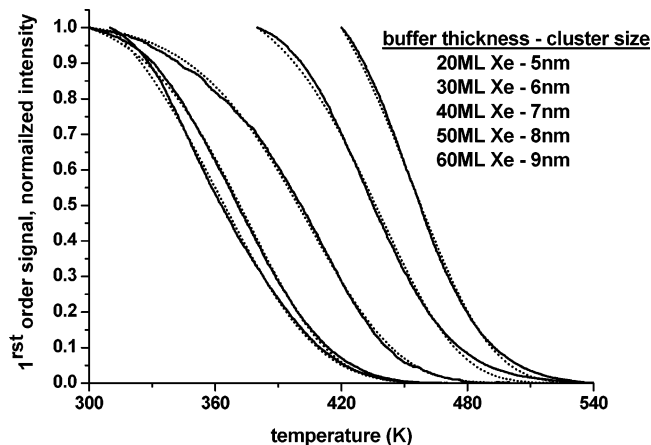


Figure 5. First-order optical linear diffraction signal from a gold coverage grating on the Ru(100) surface, at different Xe buffer thicknesses for 1 nm deposited gold, as the temperature continuously increases at 3 K/s. The dotted lines represent the best fit using eq 6; see text.

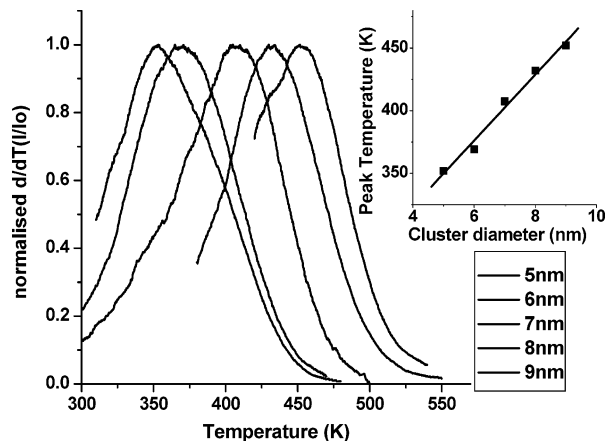


Figure 6. Normalized temperature derivative of the optical first-order linear diffraction signals of Figure 4, as a function of temperature. Inset: peak temperature as a function of the average cluster diameter.

The signal derivative will be small at low temperatures where rates are small, but will rise as the diffusion rates increase with temperature. At high temperatures, the original signal and the derivatives decrease once again because the cluster density population has been flattened, in other words the diffusion process approaches completion as the local chemical potential difference—which is the driving force for diffusion—vanishes. The signal derivative thus peaks at some intermediate temperature, which is determined by the heating rate and the diffusion kinetic parameters—higher activation energy for diffusion shifts the peak to higher temperatures. The results of this analysis are demonstrated in Figure 6 for the diffusion of several gold cluster sizes on the clean Ru(100) surface. The inset shows the peak temperature as a function of clusters average diameter. It is possible to gain further insight from eq 7. By dividing the derivative by the original signal intensity, one obtains the following:

$$B = \frac{\frac{\partial(I/I_0)}{\partial T}}{(I/I_0)} = -\frac{aD_0}{\beta} \cdot e^{-E_a/RT} \quad (8)$$

$$\ln(-B) = \ln\left(\frac{aD_0}{\beta}\right) - \frac{E_a}{R} \cdot \frac{1}{T} \quad (9)$$

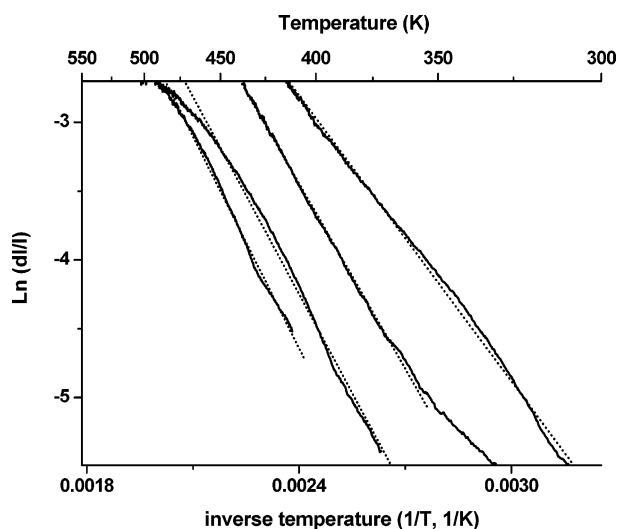


Figure 7. Natural logarithm of dI/I (the signal derivative divided by the original first-order linear diffraction signal) vs the inverse temperature. An activation energy is extracted from each line using a linear fit.

Finally, plotting the natural logarithm of $(-B)$ vs $1/T$, the activation energy can be isolated independent of the preexponent. This analysis is demonstrated in Figure 7 for the data presented in Figure 5. The main advantage of this procedure is the continuous set of data points extracted from a single measurement, covering nearly the entire temperature range. It is possible to compare the results of the procedure in eq 9 to the numbers extracted from “direct” line shape analysis. The results are very similar within the experimental error. Moreover, based on Figure 7, one can input the activation energy into the fit presented in Figure 5 to extract the preexponents.

This temperature-programmed diffusion method (TPDiff) has several advantages. It can be applied best for rate measurements that rapidly change with temperature. For example the temperature range for the diffusion process of gold clusters on the Ru substrate (about 250 K) requires a more efficient method than the conventional isothermal mode. Finally, in the case of heterogeneous processes that are characterized by a distribution of activation barriers, the TPDiff method has the potential to isolate and define this diffusion barrier distribution. In particular this is the situation in the case of the soft deposition of gold clusters via BLAG, where metallic clusters size cover a range of 20% around its average diameter.

3.4. Gold Clusters Diffusion on the Ru(100) Surface. The diffusion of size selected gold clusters on the clean Ru(100) substrate was measured by optical linear diffraction from a coverage grating, using the combined BLALP and TPDiff methods described above. The heating rate was fixed at 3 K/s at the temperature range 100–800 K. The decay of the first order optical linear diffraction signal is shown in Figure 5, normalized to its initial intensity at 100 K. The gold quantity initially evaporated on the ruthenium substrate was the equivalent of 1 nm thickness.

The onset temperature for micrometer range cluster mobility was found to be relatively low, beginning at 300 K for the smallest clusters. However, lower temperature mobility at the nanometer length scale that is not detectable by the optical diffraction method cannot be ruled out. The observed diffusion temperature range increases with the average cluster size. Line shape analysis using eq 4 above was used together with the fitting of the Arrhenius-like plot of Figure 7 to determine the activation energy and preexponential factor for diffusion of the

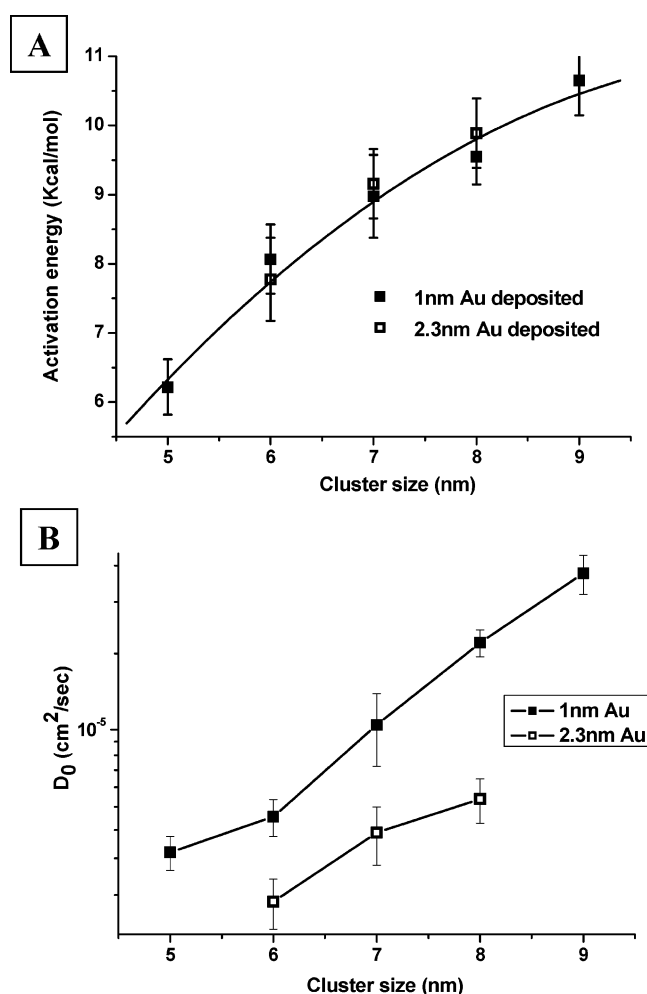


Figure 8. Activation energy (A) and preexponent (B) for the diffusion of gold clusters on the Ru(100) surface. The filled squares represent the data for 1 nm deposited gold, and the open squares for 2.3 nm deposited gold, at the indicated average cluster diameter. The lines serve as guide to the eye.

gold nanoclusters on the Ru(100) surface. The discrepancies of the fit from the experimental lines observed at the onset and termination of the diffusion process probably originate from the cluster size distribution. This becomes more pronounced with increasing cluster size, as the fwhm of the size distribution increases accordingly. This results in the more pronounced curvature of the Arrhenius plot at the beginning and the end of the temperature range. In extreme cases, the Arrhenius-like curve cannot be linearly fitted anymore, and the dependence of activation energy on cluster diameter has to be taken into account. Alternatively, the linear fit gives the activation energy for an average cluster size, for each curve.

The resulting size dependent activation energy and preexponential factor for diffusion of the metallic gold nanoclusters are summarized in Figure 8. Each point in the graph represents an average value obtained following three independent measurements for each average cluster size. The activation energy increases with the average cluster size, from 6.2 ± 0.5 kcal/mol for 5 nm clusters, to 10.6 ± 0.6 kcal/mol for 9 nm clusters. On the other hand, the preexponential factor also increases by an order of magnitude from $(3.8 \pm 0.5) \times 10^{-6}$ to $(3.4 \pm 0.5) \times 10^{-5}$ cm²/s with increasing cluster size. This however may be affected by the cluster density on the surface as will be discussed below.

The second Fick equation for diffusion described in eq 1 is valid only for non interacting adsorbates on surfaces. It is in

fact a simplification of the more complex and nonanalytically solvable equation below:

$$\frac{\partial \theta}{\partial t} = \frac{\partial}{\partial x} \left(D[\theta(x)] \frac{\partial \theta(x)}{\partial x} \right) \quad (10)$$

Equation 1 does not therefore suit for the measurement of systems where adatoms interactions cannot be neglected. To further check the validity of eq 1, the same diffusion measurements were performed at a higher cluster density, retaining the same cluster size. This can be achieved via interplay between deposited gold atoms flux and the buffer layer thickness. The results are demonstrated for 2.3 nm equivalent deposited gold on the Xe buffer layer relative to 1 nm equivalent gold on the same substrate. From a comparison of the activation energy for diffusion on both gold densities, it does not seem to significantly depend on cluster density on the surface. On the basis of this experimental observation, we have continued to analyze the cluster diffusion process using eq 1, ignoring possible (minor) interaction among neighbor clusters. There is however a difference in the temperature range in which the clusters at different densities diffuse, which is embedded in the preexponential factor, as seen in Figure 8. The preexponent is smaller by a factor of 2 in the case of the high density clusters than for the lower density ones. Qualitatively, one may explain this behavior by a “steric effect”, where clusters “collide” with each other at diffusion temperatures, effectively leading to site blocking. This slows down the overall diffusion process while decreasing the preexponent. This should not affect the activation energy for diffusion, as the clusters do not otherwise interact with each other.

As discussed above, the clusters diffuse but they do not coalesce, regardless of size or density. On the clean metallic substrate one would have expected the clusters to wet the surface, as predicted by relative surface tension values.⁶³ In most cases layer by layer growth would be the dominant mechanism at substrate temperatures above 500K. No coalescence or wetting phenomena were detected up to annealing temperatures of 650K in a vacuum, however the clusters diffuse on the surface already at temperatures as low as 350 K. The wide temperature range recorded for the macroscopic process arises from low apparent activation barrier for clusters diffusion which is smaller than the barrier for 2D evaporation of atoms from clusters edges. Both the activation energy and the preexponent for clusters diffusion are strongly cluster size dependent. When compared to evaporation renucleation processes, larger clusters on metallic surfaces tend to be more stable; therefore, they are expected to diffuse at higher temperatures.

The weak interaction between the gold nanoclusters and the Ru(100) surface is likely to be a contributing factor. The gentle deposition mechanism of the nanoclusters on top of the substrate's surface, typical to BLAG,^{27,28a} apparently leads to clusters whose barrier for diffusion is lower than for evaporation and surface wetting. Those clusters are not strongly bound to the substrate, and they diffuse rather than melt to form a uniform film on the substrate or coalescence with neighbor gold clusters. The softly deposited clusters do not anchor to the substrate, allowing its relatively free migration. As a result 2D evaporation followed by renucleation is unlikely to be the dominant mechanism in the case of gold cluster macroscopic diffusion—migration on Ru(100).

On the other hand, in order for the clusters to conserve their metastable morphology, the sintering/coalescence rate must be slow in the temperature range 300–600 K. Coalescence is expected to be observable in the presently studied system,

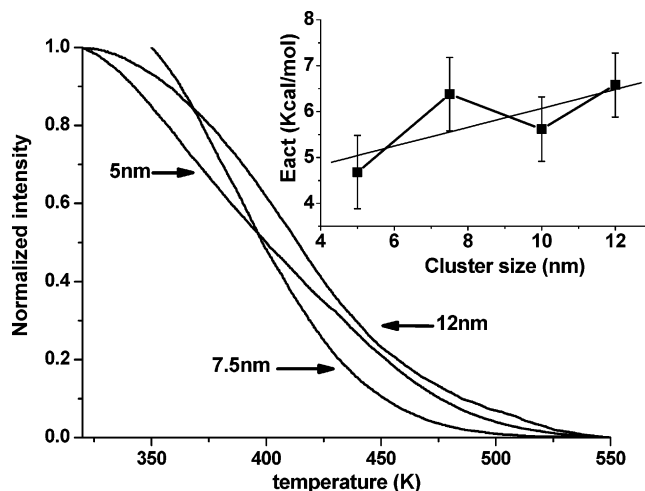


Figure 9. First-order diffraction signal decay from a gold coverage grating on the oxygen covered $p(1 \times 2)\text{-O/Ru}(100)$ substrate. Gold quantity deposited is 1 nm. Inset: activation energy for diffusion as a function of cluster size.

especially due to the relatively high density of clusters on the surface. The diffusion of clusters as a whole is somewhat surprising, however it is consistent with several recent reports of size selected deposited nanoclusters of Au,⁶⁸ Ag,⁶⁹ and Co⁷⁰ on smooth surfaces. For example, small Ag clusters on HOPG were shown to coalesce fast at room temperature,⁶⁹ while for clusters above a limit of 5 nm diameter, the rate of coalescence dramatically decreased, although cluster diffusion is clearly observed. The high dependence of cluster sintering and coalescence rate on cluster size is tentatively explained by the increasing surface melting temperature of the cluster with its size;⁷⁰ however, a more detailed study using, i.e., STM is necessary in order to propose a probable model.

3.5. Gold Cluster Diffusion on the $p(1 \times 2)\text{-O/Ru}(100)$ Surface. To better understand the role of the substrate on the thermal stability of the gold clusters, their diffusion has also been measured on the oxygen covered surface of Ru(100). It may be considered as a model for supported clusters on oxide surfaces. The Ru(100) surface transforms into a well ordered $p(1 \times 2)\text{-O}$ lattice, as observed by a sharp LEED pattern.^{64–66} The diffusion characteristics of the gold clusters on the oxygen covered surface are similar to that on the bare Ru(100) surface, as deduced from AFM measurements; namely, clusters diffuse over macroscopic distances intact with practically no sintering or coalescence. The decay of the first-order linear diffraction signal reflects the identical procedure of BLALP-TPDiff as described for the clean Ru(100) surface. Diffusion measurements were performed for clusters between 5 and 12 nm in diameter, using 1 nm Au and 20–105ML Xe. The resulting optical diffraction decay spectra and their respective energy barrier as a function of cluster size are shown in Figure 9. The diffusion takes place at temperatures between 350 and 550 K, about the same as for the diffusion on the clean Ru(100) surface. However, unlike the clean Ru(100) substrate, only minor dependence on cluster size has been observed in these measurements, and the activation energy is observed to be only slightly increasing with the cluster size. One may consider the activation energy for diffusion on $p(1 \times 2)\text{-O/Ru}(100)$ as a constant value of 5.5 ± 1 kcal/mol. The preexponential factor reveals similar lack of sensitivity to cluster size, its value being $(1 \pm 2) \times 10^{-6} \text{ cm}^2/\text{s}$.

The diffusion mechanism over the oxygen covered ruthenium seems to be similar to diffusion on the clean surface. Oxygen

covers only the topmost layer of the metallic substrate; therefore, it does not behave like a bulk-oxide surface. However, the fact that clusters as large as 12 nm in diameter diffuse with practically the same activation energy as small clusters (5 nm diameter) suggests that on top of the oxygen-covered surface, the interaction between the clusters and the supporting substrate is rather weak.

This behavior may be qualitatively explained in terms of commensurability between the cluster surface and the substrate lattice. The deposited clusters do not form any anchor to the oxygen covered substrate, as would be expected for clusters directly grown over an oxide surface.⁶⁴ Moreover, the ordered $p(1 \times 2)$ -O/Ru(100) surface is expected to have a much smaller density of defect sites than oxides grown as layers on top of a metallic substrate^{4,7,8,15} or as bulk.¹ As a result they relatively easily slide on the surface, similar to the gold clusters deposited on the bare Ru(100). This result further demonstrates the kinetic stability of BLAG deposited clusters over those grown directly on the surface. The lower activation energy is then proposed to arise from the oxygen atoms adsorbed on the surface acting as a “buffer” between the cluster and the metallic substrate, inducing an effective smoothing of the ruthenium atomic rows along the [001] direction, further reducing the commensurability of the gold clusters. The oxygen covered surface serves only as a non interacting support, and the free energy involved permits diffusion with a lower barrier, as compared to atomic diffusion on the surface of the metallic clusters or/and the substrate. This hypothesis is supported by the observation that diffusion takes place already at remarkably low temperatures considering expectations for very large 3D metallic clusters. This may explain why the diffusion barrier is so insensitive to cluster size.

Conclusions

The BLAG method allows the formation and deposition of size selected clusters regardless of the underlying substrate. The BLALP procedure enables the formation of cluster coverage modulation on surfaces, and it is a template for the study of macroscopic diffusion of metallic clusters on surfaces. The diffusion of gold nanoclusters on the Ru(100) and the $p(1 \times 2)$ -O/Ru(100) oxygen covered surface has been measured as a function of the cluster size. This study presents the first direct measurement of nanometer scale metal clusters mobility on metallic and oxide-like surfaces over macroscopic distances (micrometer range). A new procedure for the analysis of surface diffusion—temperature-programmed diffusion (TPDiff) has been introduced for this purpose. On both surfaces, the diffusion process has been of intact clusters, with practically no coalescence or sintering phenomena up to temperatures of 600 K. Cluster diffusion can be described by the one-dimensional, second Fick equation for diffusion on the macroscopic scale, and it exhibits Arrhenius temperature dependence. The activation energy for diffusion was found to be sensitive to the cluster size on the clean Ru(100) surface. However, on the $p(1 \times 2)$ -O/Ru(100) substrate, no cluster size dependence was found. This surprising result may be explained by the lack of commensurability of the gold metallic clusters on the oxygen covered surface and the very weak interaction of the clusters with the substrate.

The results of this study suggest a different behavior of BLAG grown vs directly grown clusters on surfaces for clusters larger than 5 nm diameter. Intact cluster diffusion seems to be the dominant process for BLAG grown clusters with only minor cluster morphology changes and coalescence/sintering, limited

to clusters smaller than 5 nm diameter. It suggests that clusters prepared in this way may be more stable under realistic high-pressure–high-temperature conditions typical for the industrial environment.

Acknowledgment. This work was partially supported by a grant from the US–Israel Binational Science Foundation and the Israel Science Foundation. The Farkas center is supported by the Bundesministerium für Forschung und Technologie and the Minerva Gesellschaft für die Forschung mbh.

References and Notes

- (1) Henry, C. R. *Surf. Sci. Rep.* **1998**, *31*, 231.
- (2) Binns, C. *Surf. Sci. Rep.* **2001**, *44*, 1.
- (3) Freund, H. J. *Angew. Chem., Int. Ed. Engl.* **1997**, *36*, 452.
- (4) Campbell, C. T. *Surf. Sci. Rep.* **1997**, *27*, 1.
- (5) Schumacher, E. *Chimia* **1988**, *42*, 357.
- (6) Bäumer, M.; Freund, H. J. *Prog. Surf. Sci.* **1999**, *61*, 127.
- (7) Street, S. C.; Xu, C.; Goodman, D. W. *Annu. Rev. Chem.* **1997**, *48*, 43.
- (8) Goodman, D. W. *J. Catal.* **2003**, *216* (1–2), 213.
- (9) Chusuei, C. C.; Lai, X.; Luo, K.; Goodman, D. W. *Top. Catal.* **2001**, *14* (1–4), 71.
- (10) Choudhary, T. V.; Goodman, D. W. *Top. Catal.* **2002**, *21* (1–3), 25.
- (11) Sandell, A.; Libuda, J.; Bäumer, M.; Freund, H. J. *Surf. Sci.* **1996**, *346*, 108.
- (12) Goodman, D. W. *J. Phys. Chem.* **1996**, *100*, 13090.
- (13) Rainer, D. R.; Xu, C.; Goodman, D. W. *J. Mol. Catal. A: Chem.* **1997**, *119*, 307.
- (14) Street, S. C.; Xu, C.; Goodman, D. W. *Annu. Rev. Phys. Chem.* **1997**, *48*, 43.
- (15) Goodman, D. W. *Chem. Rev.* **1995**, *95*, 523.
- (16) Haruta, M. *Catal. Today* **1997**, *36*, 153.
- (17) Valden, M.; Lai, X.; Goodman, D. W. *Science* **1998**, *281*, 1647.
- (18) Ajo, H. M.; Bondzie, V. A.; Campbell, C. T. *Catal. Lett.* **2002**, *78* (1–4), 359.
- (19) Sanchez, A.; Abbet, S.; Heiz, U.; Schneider, W.-D.; Hakkinen, H.; Varnett, R. N.; Landman, U. *J. Phys. Chem. A* **1999**, *103*, 9573.
- (20) Bond, G. C. *Catal. Today* **2002**, *72*, 5–9.
- (21) Luo, K.; Kim, D. Y.; Goodman, D. W. *J. Mol. Catal. A: Chem.* **2001**, *167*, 191.
- (22) Santra, A. K.; Min, B. K.; Goodman, D. W. *Surf. Sci.* **2002**, *515*, L475.
- (23) Bauer, E. Z. *Kristallogr.* **1958**, *110*, 372.
- (24) Waddill, G. D.; Vitomirov, I. M.; Aldao, C. M.; Weaver, J. H. *Phys. Rev. Lett.* **1989**, *62*, 1568.
- (25) Huang, L.; Chey, S. J.; Weaver, J. H. *Phys. Rev. Lett.* **1998**, *80*, 4095.
- (26) Huang, L.; Chey, S. J.; Weaver, J. H. *Phys. Rev. B* **1999**, *59*, 16033.
- (27) Antonov, V. N.; Weaver, J. H. *Surf. Sci.* **2003**, *526*, 97.
- (28) (a) Haley, C.; Weaver, J. H. *Surf. Sci.* **2002**, *518*, 243. (b) Yoo, K.; Li, A.-P.; Zhang, Z.; Weitering, H. H.; Flack, F.; Lagally, M. G.; Wendelken, J. F. *Surf. Sci.* **2003**, *546*, L803. (c) Pierce, J. P.; Torija, M. A.; Gai, Z.; Shi, J.; Schulthess, T. C.; Farnan, G. A.; Wendelken, J. F.; Plummer, E. W.; Shen, J. *Phys. Rev. Lett.* **2004**, *92*, 237201.
- (29) Antonov, V. N.; Palmer, J. S.; Bhatti, A.; Weaver, J. H. *Phys. Rev. B* **2003**, *68*, 205418.
- (30) Antonov, V. N.; Palmer, J. S.; Waggoner, P. S.; Bhatti, A.; Weaver, J. H.; *Phys. Rev. B* **2004**, *70*, 045406.
- (31) Zhu, X. D.; Rasing, Th.; Shen, Y. R. *Phys. Rev. Lett.* **1988**, *61*, 2883.
- (32) Xiao, X. D.; Xie and Shen, Y.; Y. R. *Surf. Sci.* **1992**, *271*, 295.
- (33) Burgess, D., Jr.; Stair, P. C.; Weitz, E. J. *J. Vac. Sci. Technol. A* **1986**, *4*, 1362.
- (34) Rosenzweig, Z.; Asscher, M. *J. Chem. Phys.* **1992**, *96*, 4040.
- (35) Zhu, X. D.; Rasing, Th.; Shen, Y. R. *Phys. Rev. Lett.* **1988**, *61*, 2883.
- (36) Xiao, X. D.; Xie and Shen, Y.; Y. R. *Surf. Sci.* **1992**, *271*, 295.
- (37) Gomer, R. *Rep. Prog. Phys.* **1990**, *53*, 917.
- (38) Zhu, X. D. *Modern Phys. Lett. B* **1992**, *6*, 1217.
- (39) Zhu, X. D.; Lee, A.; Wong, A. *Appl. Phys. A: Mater. Sci. Process.* **1991**, *52*, 317.
- (40) Zhu, X. D.; Lee, A.; Wong, A. *Phys. Rev. Lett.* **1992**, *68*, 1862.
- (41) Zhao, W.; Kerner, G.; Asscher, M.; Wilde, M.; Al-Shamry, K.; Freund, H.-J.; Staemmler, V.; Wieszbowska, M. *Phys. Rev. B* **2000**, *62*, 7527.
- (42) Kerner, G.; Danziger, I. M.; Zhao, W.; Asscher, M. In *NATO Advanced Research Workshop on “Collective Surface Diffusion Coefficients*

Under Non -Equilibrium Conditions"; Tringides, M., Chevoj, Z., Eds.; Kluwer Academic Publishers: Dordrecht, The Netherlands, 2000.

(43) Zhao, W.; Asscher, M. *Surf. Sci.* **1999**, *429*, 1.

(44) Zhao, W.; Verhoef, R. W.; Asscher, M. *J. Chem. Phys.* **1997**, *107*, 5554.

(45) Kerner, G.; Asscher, M. *Surf. Sci.* **2004**, *557*, 5.

(46) Kerner, G.; Asscher, M. *Nano Lett.* **2004**, *4*, 1433.

(47) Schlichting, H.; Menzel, D. *Rev. Sci. Instrum.* **1993**, *64*, 2013.

(48) Smentkowski, V. S.; Yates, J. T., Jr. *J. Vac. Sci. Technol. A* **1996**, *14*, 260.

(49) Grunze, M. Ruppender, H.; Elshazly, O. *J. Vac. Sci. Technol. A* **1988**, *6*, 1266.

(50) Kerner, G.; Stein, O.; Lilach, Y.; Asscher, M. Submitted for publication.

(51) Berendzen, J.; Braunseint, D. *Proc. Natl. Acad. Sci. U.S.A.* **1990**, *87*, 1.

(52) Goldstein, J. T.; Ehrlich, G. *Surf. Sci.* **1999**, *443*, 105.

(53) Wang, S. C.; Ehrlich, G. *Phys. Rev. Lett.* **1997**, *79*, 4234.

(54) Kellogg, G. L. *Prog. Surf. Sci.* **1996**, *53*, 217.

(55) Gastel, R. V.; Plass, R.; Bartelt, N. C.; Kellogg, G. L. *Phys. Rev. Lett.* **2003**, *91*, 055503.

(56) Felix, C.; Vandoni, G.; Harbich, W.; Buttet, J.; Monot, R. *Phys. Rev. B* **1996**, *54*, 17039.

(57) Pai, W. W.; Swan, A. K.; Zhang, Z.; Wendelken, J. F. *Phys. Rev. Lett.* **1997**, *79*, 3210.

(58) Wen, J.-M.; Evans, J. W.; Bartelt, M. C.; Burnett, J. W.; Thiel, P. A. *Phys. Rev. Lett.* **1996**, *76*, 652.

(59) Carrey, J.; Maurice, J.-L.; Petroff, F.; Vaures, A. *Phys. Rev. Lett.* **2001**, *86*, 4600.

(60) Gan, S.; El-azab, A.; Liang, Y. *Surf. Sci.* **2001**, *479*, L369.

(61) El-azab, A.; Gan, S.; Liang, Y. *Surf. Sci.* **2002**, *506*, 93.

(62) AFM images were measured with a DI 3100 nanoscope instrument, using the tapping mode with a TESP tip.

(63) Poulson, S.; Tikhov, M.; Lambert, R. M. *Surf. Sci.* **1995**, *331*–*333*, 818.

(64) Poulson, S.; Tikhov, M.; Lambert, R. M. *Langmuir* **1995**, *13*, 5356.

(65) Baraldi, A.; Lizzit, S.; Paolucci, G. *Surf. Sci.* **2000**, *457*, L354.

(66) Schwegmann, S.; Seitsonem, A. P.; De Renzi, V.; Dietrich, H.; Bludau, H.; Gierer, M.; Over, H.; Jacobi, K.; Scheffler, M.; Ertl, G. *Phys. Rev. B* **1998**, *57*, 15487.

(67) Zhuang, G.; Wang, W. *IJMPB* **2000**, *14*, 4, 427.

(68) Eastham, D. A.; Hamilton, B.; Denby, P. M. *Nanotechnology* **2002**, *13*, 51.

(69) Couillard, M.; Pratontep, S.; Palmer, R. E. *Appl. Phys. Lett.* **2003**, *82*, 2595.

(70) Peng, D. L.; Konno, T. J.; Wakho, K.; Hihara, T.; Sumiyama, K. *Appl. Phys. Lett.* **2001**, *78*, 1535.